

Article

Implementing a Precision Pneumatic Plug Tray Seeder with High Seeding Rates for Brassicaceae Seeds via Real-Time Trajectory Tracking Control

Hao-Ting Lin *  and Yu-Hsien Lee 

Department of Bio-Industrial Mechatronics Engineering, National Chung Hsing University, Taichung 402, Taiwan; yhlee@smail.nchu.edu.tw

* Correspondence: haotlin@nchu.edu.tw

Abstract: In recent years, the aging of the rural population worldwide has become a major concern, necessitating the development of agricultural automation. Pneumatic energy has emerged as a reliable and environmentally friendly option, aiding in the global effort to reduce carbon emissions. The purpose of this study is to reduce the amount of labor required for plug tray seeding by developing an automated seeder that employs a precision pneumatic servo system via the rod-less actuator with real-time trajectory tracking capabilities. The proposed seeder has a simple structure, is easy to maintain, and saves energy. It mainly consists of a rod-less pneumatic cylinder, a needle seeding mechanism, a soil drilling mechanism and a PC-based real-time controller. Mathematical models of the developed precision pneumatic plug tray seeder are analyzed and established, and an adaptive sliding mode controller is proposed. A PC-based real-time control system is developed using MATLAB/SIMULINK via an optical encoder with a sampling frequency of 1 kHz to enable the development of precise pneumatic plug tray seeder. An optical encoder is used to measure the displacement of the rod-less cylinder which represents real-time positions of the plug tray loading platform. Experiments are conducted using Brassicaceae seeds, and the rates of single seeding, multiple seeding, missed seeding and germination are carried out through manual measurement. The results indicate that the seeder exhibits satisfactory performance, with a root mean square error of less than 0.5 mm and a single-seeding rate of more than 97%. Overall, our findings provide new insights for nurseries and could contribute to the reduction in agricultural carbon emissions.

Keywords: plug tray seeder; pneumatic servo system; sliding mode control; trajectory tracking control



Citation: Lin, H.-T.; Lee, Y.-H. Implementing a Precision Pneumatic Plug Tray Seeder with High Seeding Rates for Brassicaceae Seeds via Real-Time Trajectory Tracking Control. *Actuators* **2023**, *12*, 340. <https://doi.org/10.3390/act12090340>

Academic Editors: Gary M. Bone and Hai Wang

Received: 16 June 2023

Revised: 7 August 2023

Accepted: 23 August 2023

Published: 24 August 2023



Copyright: © 2023 by the authors. Licensee MDPI, Basel, Switzerland. This article is an open access article distributed under the terms and conditions of the Creative Commons Attribution (CC BY) license (<https://creativecommons.org/licenses/by/4.0/>).

1. Introduction

Growing seedlings in plug trays is an efficient and reliable method that is often used for vegetable crops. Seeding in plug trays saves seeds, produces a large yield per unit area, induces independent seedling growth, and ensures uniform quality. In the seedling industry, manual seeding is a slow and labor-intensive process. Gaikwad and Sirohi [1] developed a low-cost pneumatic seeder and evaluated its performance using chili pepper and tomato seeds. They reported that their seeder achieved a single-seeding rate of more than 90% at approximately 15.27% of the overall cost of manual seeding. EL-Ghobashy et al. [2] proposed a continuous feeding mechanism for precision plug tray seeders and compared two plug tray types, four suction pressure levels, and four suction hole diameters for cucumber and cabbage seeding; they reported that their precision plug tray seeder resulted in 5–12-fold cost reductions compared with manual seeding. Plug trays with 104 cells are commonly used to promote the germination of many vegetable and fruit seedlings. To reduce seed waste, labor, and seeding time, Naik and Thakur [3] developed a pneumatic plug tray seeder that effectively saved 66.08% of the cost of manual seeding and required only 27.87 h of operation to recover the seeder cost. To monitor seeder performance and ensure seeding quality, Xia et al. [4] established a photoelectric measurement

system using a row of fiber-optic sensors on a pneumatic roller seeder, and evaluated its performance using 10 vegetable seeds; they reported that their system precisely determined the corresponding single-seeding, missed-seeding, and multiple-seeding rates. Theoretically, optimal seeding parameters strongly correlate with the physical properties of seeds. Karayel et al. [5] developed a mathematical model of seeder vacuum pressure to determine the optimal vacuum pressure for seed suction depending on the physical properties of the seeds; they also established a mathematical model for prediction. Xia et al. [6] proposed an optimization method for determining the operational parameters of roller seeders; they used collections of similar seeds to predict optimal operating conditions through particle swarm optimization algorithms, which can be applied to real-life seeding scenarios. To improve the performance of pneumatic precision seeders, Pareek et al. [7] combined an artificial neural network method and a multiobjective particle swarm optimization method to determine the optimal hole shape, hole size, vacuum pressure, and operating speed. Li et al. [8] developed a pneumatic rapeseed seeder. In order to improve seeding performances, they simulated and evaluated the suction hole shape, hole diameter and flow field effects with a high-speed camera. They reported that their seeder achieved a missed-seeding rate of less than 3% under optimal conditions.

In recent years, reducing carbon emissions and developing clean energy have become global priorities. In line with these priorities, pneumatic actuators, which generate pressure energy by compressing air, have garnered widespread attention in both industrial and agricultural applications. Compared with traditional fuel engines, hydraulics, and motors, pneumatic systems offer the advantages of being clean, cheap, safe, and easy maintenance. In addition, they align with current international policies for reducing carbon emissions and improving energy efficiency. However, pneumatic systems exhibit compressibility, dead zones, zero drift, and other phenomena, all of which make them highly nonlinear and difficult to control with precision. Therefore, achieving precise pneumatic control requires the use of servo systems and careful controller design. Valdiero et al. [9] developed a mathematical model for a servo pneumatic actuator and proposed a fifth-order nonlinear mathematical model that includes the primary characteristics of nonlinear dynamic systems; they also investigated the dynamic performances of multiple cylinders through simulation, which enabled them to achieve precise control of pneumatic actuators. Moriwaki [10] developed a pneumatic automatic cart which is used for harvesting. The harvesting vehicle can maintain the level of the loading platform while driving on rugged farm roads. Pneumatic servo systems have the potential to replace hydraulic and electromechanical systems. Lin et al. [11] applied position feedback dynamic surface control to pneumatic systems and developed an improved dynamic surface controller to overcome model uncertainty, external disturbances, and noise interference; they verified through experiments that the proposed control method exhibited more advantages than traditional proportional–integral–derivative (PID) controllers. Zhang et al. [12] proposed an accurate model for a valve controlled pneumatic rotary actuator servo system. The characteristics equations are derived precisely with the mass flow rate and the Stribeck friction method. To address environmental concerns, Gao et al. [13] proposed an integrated mechanized operation solution and explored the use of PID controllers and soft computing optimization methods to control the positions of servo motors and pneumatic servo systems; according to their simulation findings, the suggested control approach demonstrated precise position results, exhibiting errors of less than 20 mm. This achievement can be applied for ship rust removal and painting processes. Precise pneumatic control heavily relies on a well-designed proportional servo valve. Zhang et al. [14] proposed positioning strategies based on parameter tuning and optimization control techniques to enhance the accuracy, speed, and versatility of pneumatic control valves. This approach shortened the system adjustment time and improved valve position accuracy. Wang et al. [15] established a finite element dynamic mathematical model and conducted finite element analysis on the magnetic field inside a pneumatic proportional servo valve; they optimized the valve through analysis, thereby reducing the hysteresis phenomenon within the working pres-

sure range and achieving high performance for step signals. Zhu et al. [16] introduced a fractional-order model for the pneumatic control valve. The experiments demonstrated excellent adaptability and effectiveness for position control.

Sliding mode control (SMC) is extensively used in nonlinear control systems and is known for its robustness. Ding et al. [17] developed a novel second-order SMC algorithm for output-constrained problems by constructing a new barrier Lyapunov function and applying the technique of adding power integrators; their proposed algorithm ensured that the output variable remained within the boundary of the constraint region, whereas the sliding variable could be stabilized to zero within a finite period. Fei et al. [18] devised an adaptive fractional order sliding mode controller for a micro-gyroscope and a dual-loop recursive fuzzy neural network to approximate uncertainties and disturbances of the system; their simulation results indicated that the proposed control strategy exhibited excellent performance in terms of trajectory tracking control. Li et al. [19] proposed a fuzzy SMC technique based on a saturation function for a pneumatic muscle actuator to simulate the actual motion of the human upper arm; they used fuzzy control and saturation function adjustment for a robust term to improve tracking accuracy, reduce high-frequency oscillations, and achieve excellent performance in trajectory tracking experiments. Yu et al. [20] investigated and analyzed seven SMC methods, the boundary layer method, the reaching law method, SMC based on a disturbance observer, terminal SMC, hypertwisting SMC, adaptive SMC, and intelligent SMC. Chen et al. [21] developed an improved sliding mode controller with active disturbance rejection to enhance the vertical stability of unmanned ground vehicles, coupled with an extended state observer to estimate disturbances arising from the model's nonlinear height and uncertainty; they validated the effectiveness of the proposed controller and its robustness to load parameter uncertainty through simulations. Sun et al. [22] presented a fuzzy adaptive recursive terminal sliding mode control technique for an agricultural omnidirectional mobile robot to balance tracking accuracy and control smoothness. Kinematic and dynamic models comprise four control inputs and three states. They reported that the proposed control strategy successfully completed a trajectory tracking task in agricultural product transportation.

In this study, we reviewed previous studies regarding the development of pneumatic seeders, pneumatic systems, and control technologies. Using the software SolidWorks developed by Dassault Systems, we designed a precision pneumatic plug tray seeder with a rod-less pneumatic cylinder and a pneumatic servo system, which achieved more precise seeding compared with traditional motor-powered methods. Optical encoders are used to precisely measure positions of the plug tray loading platform. We also established dynamic models for the developed pneumatic system and conducted adaptive sliding mode control simulations on MATLAB. In addition, we used MATLAB/SIMULINK to establish a PC-based real-time trajectory tracking control environment. The performances of the proposed controller were analyzed by comparing various control methods [23,24]. We then evaluated the developed pneumatic seeder using multiple cruciferous seeds to achieve precise seeding.

This paper is organized as follows: In Section 1, the research background and a review of the relevant literature concerning plug tray seeding and pneumatic systems are introduced. Section 2 outlines the experimental methods and materials used to develop the precision pneumatic plug tray seeder. Section 3 presents the established mathematical models and the design of an adaptive sliding mode controller for the seeder. In Section 4, simulation and experimental results are presented for evaluating the seeder's performance in seeding and germination. Finally, Section 5 summarizes the achievements of the precision pneumatic plug tray seeder.

2. Experimental Method

2.1. Structural Design of the Precision Pneumatic Plug Tray Seeder

In this study, a precision pneumatic plug tray seeder was developed to automate the seeding process in plug trays. As shown in Figure 1, the precision pneumatic plug

tray seeder contained a plug tray loading platform, a soil drilling mechanism, a needle seeding mechanism, and a seed groove. It also contained a rod-less pneumatic cylinder, an auxiliary pneumatic cylinder, a pneumatic servo valve, guided drives, solenoid valves, vacuum generators, and an optical encoder. These components formed a reciprocating conveying mechanism that enabled automatic seeding in plug trays. Figure 2 shows the suction needles with inner diameters of 0.21, 0.26, 0.33, 0.41, 0.51, 0.6, 0.65 and 0.84 mm which were used for the experiments.

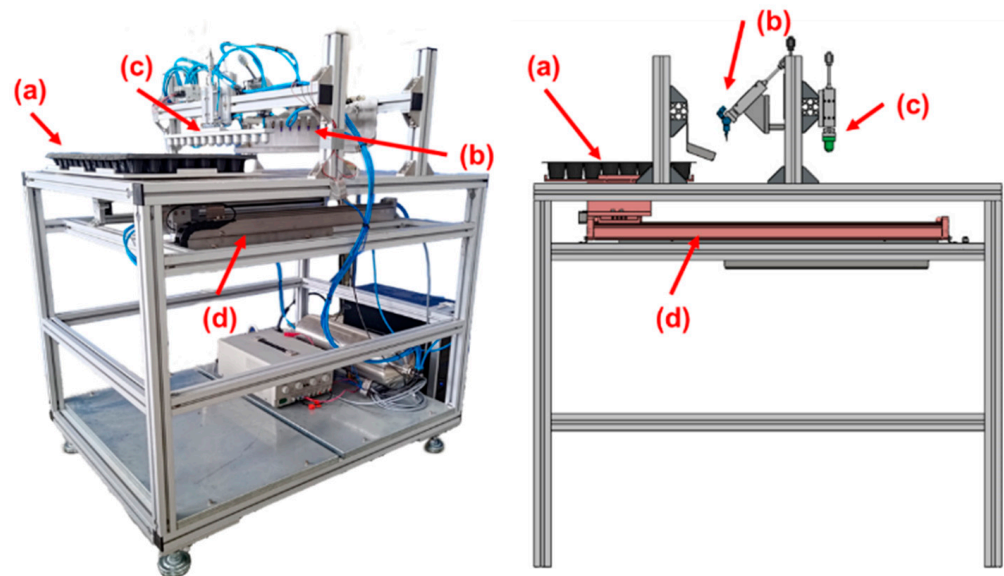


Figure 1. Structure of the precision pneumatic plug tray seeder: (a) plug tray loading platform; (b) needle seeding mechanism; (c) soil drilling mechanism; (d) rod-less pneumatic cylinder.



Figure 2. Suction needles with inner diameters of 0.21, 0.26, 0.33, 0.41, 0.51, 0.6, 0.65 and 0.84 mm were used for experiments.

2.2. Precision Pneumatic Plug Tray Seeder Layout and Real-Time Control System

Figure 3 shows the layout of the precision pneumatic plug tray seeder and the PC-based real-time control system, which was developed using MATLAB/SIMULINK R2018b. Both the rod-less pneumatic actuator (model DGC-18-700-GF-PPV-A) and the auxiliary cylinder (model DGC-18-700-FA-P), with a stroke of 700 mm, were manufactured by Festo in Germany. The proportional directional control valve (model MPYE-5-1/8-HF-010-B; Festo, Germany) was used to control the rod-less actuator. Input voltages of a pneumatic valve was set to 0–10 V, with a median voltage of 5 V. Three guided drives (DFM-12-50-B-P-A-GF-AJ; Festo, Germany) with a stroke of 50 mm were used to drive the soil drilling and needle seeding mechanisms. Solenoid valves (VUVG-L14-M52-AT-G18-1P3; Festo, Germany) were used to control the aforementioned guided drives. Three vacuum generators (VN-10-L-T3-PQ2-VQ2-RO1-B; Festo, Germany) were used to provide a negative pressure for the needle seeding mechanism through needles with a length of 30 mm, an internal diameter of 0.51 mm, and an external diameter of 0.82 mm. Figure 4 demonstrates

vacuum P_u as a function of operating pressure P_1 . The relationship between vacuum P_u and operating pressure P_1 for vacuum generators that we adopted is line 9. So, in the operating pressure set at 6 bar, vacuum generators can produce a negative pressure of -0.6 to -0.7 bar. An optical encoder (model LIA20; Numerik Jena, Jena, Germany) was used to determine the position of the plug tray loading platform according to the receiver module which receives the A and B phase signals with a phase difference of 90 degrees to determine the relationships between the A and B phases for directions of object movement.

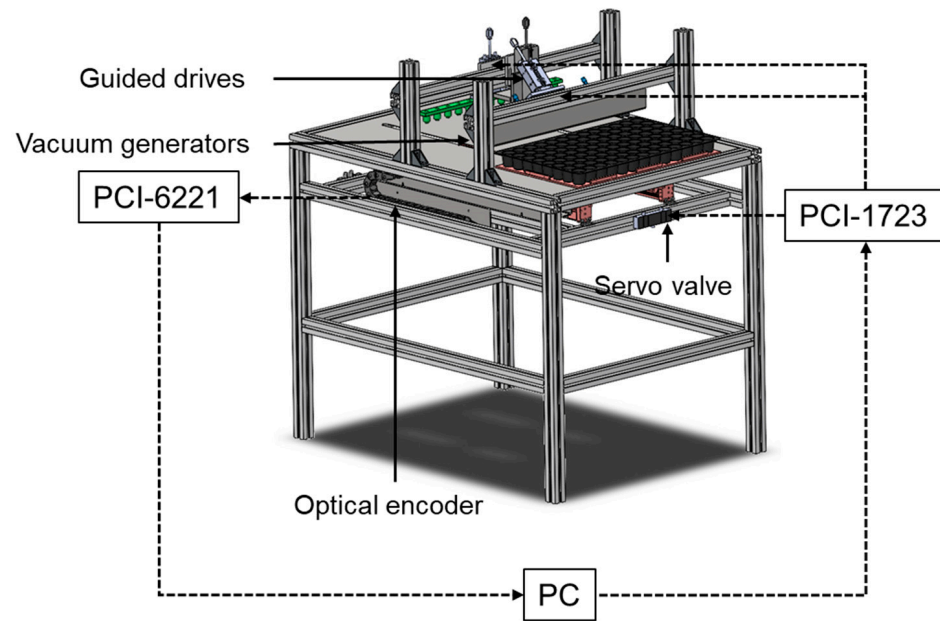


Figure 3. Layout of the precision pneumatic plug tray seeder and the PC-based real-time control system.

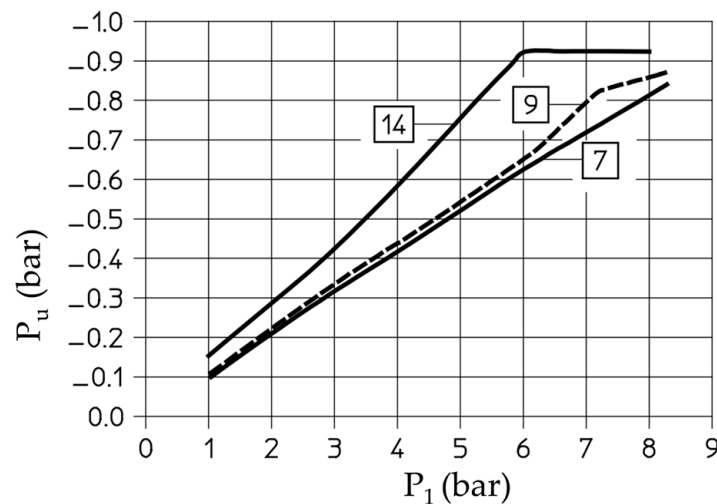


Figure 4. Vacuum P_u as a function of operating pressure P_1 [25].

During signal transmission, a data acquisition (DAQ) card (PCI-1723; Advantech, Taipei, Taiwan) was used to control the signals of the proportional directional control valve, solenoid valves, and vacuum generators. A counter card (PCI-6221; National Instruments, Austin, TX, USA) with a sampling frequency of 1 kHz was used to collect the feedback signals of the optical encoder. Therefore, the position of a plug tray loading platform can be obtained by counting the output pulses via a counter card. To drive the rod-less pneumatic cylinder through the DAQ card, the control signals generated with MATLAB/SIMULINK

were transmitted to the pneumatic servo valve. Subsequently, the displacements of the cylinder were collected via the optical encoder and fed back to MATLAB/SIMULINK through the counter card, and the reference trajectories were then compared to realize real-time control. Because of the reasonable design of the controller and the continuous correction of tracking errors, the plug tray loading platform was able to reach the designated position with precision. Table 1 shows the specifications of the precision pneumatic plug tray seeder and the PC-based real-time control system.

Table 1. Specifications of the precision pneumatic plug tray seeder and the PC-based real-time control system.

Component	Specification
Rod-less pneumatic actuator	Piston diameter: 18 mm Stroke: 700 mm
Auxiliary cylinder	Stroke: 700 mm
Guided drive	Piston diameter: 12 mm Stroke: 50 mm
Pneumatic servo valve	5/3-way function Input voltage: 0–10 V
Solenoid valve	5/2-way function
Vacuum generator	2/3-way function
Optical encoder	Range: 700 mm Resolution: 1 μ m
DAQ card	16-bit, 8-ch., non-isolated analog output card Output range: ± 10 V, 0–20 mA, 4–20 mA
Counter card	Analog I/O, correlated digital I/O, two 32-bit counters/timers, and digital triggering
Needle	Inside diameter: 0.51 mm Outside diameter: 0.82 mm Length: 30 mm
Plug tray	104 cells, 42 mm for cell diameter

2.3. Experimental Setup

Experiments were conducted on the precision pneumatic plug tray seeder using 104-cell plug trays and cruciferous seeds, whose properties are listed in Table 2. Seeder performance was evaluated by measuring the single-seeding, multiple-seeding, and missed-seeding rates. Displacement of the plug tray loading platform was measured using an optical encoder, and system performance was evaluated using the root mean square error (RMSE) and single-seeding rate.

Table 2. Properties of cruciferous seeds.

Crop	Length (mm)	Width (mm)	Aspect Ratio	Weight of 1000 Seeds (g)
<i>Brassica rapa</i> subsp. <i>pekinensis</i>	1.977 \pm 0.133	1.713 \pm 0.124	1.154	3.27
<i>Brassica rapa</i> subsp. <i>chinensis</i>	1.969 \pm 0.119	1.727 \pm 0.119	1.140	3.43
<i>Brassica parachinensis</i>	1.902 \pm 0.112	1.668 \pm 0.090	1.292	2.41
<i>Brassica oleracea</i> var. <i>botrytis</i>	1.792 \pm 0.130	1.509 \pm 0.099	1.188	1.74
<i>Brassica oleracea</i> var. <i>capitata</i>	2.505 \pm 0.183	2.088 \pm 0.201	1.200	4.39

3. Mathematical Model and Controller

3.1. Mathematical Model of the Precision Pneumatic Plug Tray Seeder [26,27]

The precision pneumatic plug tray seeder developed in this study is driven by air pressure and can be precisely controlled with voltage signals that control the pneumatic

valve. However, because of the compressibility of gas, pneumatic systems exhibit strong nonlinearity, which necessitates prior simulation to ensure system validity. In this section, we describe the mathematical model established for the proposed system. The mathematical model of this system is derived from my previous studies [23,24]. More details of fluid dynamics were considered, such as the frequency response of the pneumatic servo valve and specific heat capacities of heat conduction in the Mayer's equation. Figure 5 shows a schematic of the rod-less cylinder with a pneumatic valve. With the motion model of the rod-less cylinder, we can derive the following equations in accordance with Newton's second law:

$$A_v(t)(P_1(t) - P_2(t))\text{sgn}(\dot{y}(t)) - F_f = m\ddot{y}(t) \quad (1)$$

$$F_f = \mu_v\dot{y}(t) + k_s y(t) + \mu_c \text{sgn}(\dot{y}(t)) + f_l \text{sgn}(\dot{y}(t)) \quad (2)$$

where A_v is the opening area of the pneumatic valve and $P_{1,2}$ is the pressure inside the chambers. In these equations, F_f is used to describe various friction forces in the rod-less pneumatic cylinder, where μ_v is the viscosity coefficient, k_s is the stiffness coefficient, μ_c is the Coulomb friction force, f_l is the external disturbance force, and m is the cylinder payload. The following equation describes the relationships between the valve-opening area A_v and the control signal u :

$$A_v(t) = K_v u(t) \quad (3)$$

where K_v is the gain constant. Figure 6 illustrates the frequency response of the pneumatic servo valve, comparing the input signal with the pressure variation, 0–6 bar. By examining the Bode diagram, the utilized control signal $u(t)$, 1 kHz, significantly exceeds the bandwidth of the pneumatic servo valve. The mass flow rate $\dot{M}_{1,2}$ of the rod-less pneumatic cylinder can be expressed as follows:

$$\dot{M}_{1,2}(t) = \frac{C_d C_m P_i}{\sqrt{T_s}} A_{v1,2}(t) + \frac{C_d C_m A_{v1,2}(t)}{\sqrt{T_s}} P_i(t) \quad (4)$$

where C_d is the displacement coefficient, C_m is the mass flow rate parameter, P_i is the working pressure, and T_s is the air source temperature. The following is the mathematical expression for the volume $V_{1,2}$ of chambers 1 and 2:

$$V_{1,2}(t) = V_i + A_{v1,2}(t)y(t) \quad (5)$$

where V_i is the initial volume and where $y(t)$ is the piston displacement. The continuity equation is used to describe the relationship between mass flow rate and pressure changes. The following is the continuity equation for chambers 1 and 2:

$$\dot{M}_1(t) + \dot{M}_2(t) = \frac{1}{RT_s} \left(2P_i A_v(t) \dot{y}(t) + \frac{V_i}{k} (\dot{P}_1(t) - \dot{P}_2(t)) \right) \quad (6)$$

$$k = \frac{C_p}{C_v} \quad (7)$$

where R is the ideal gas constant, k is the specific heat, and C_p and C_v are the specific heat capacities at constant pressure and constant volume, respectively, which are related through the Mayer's equation, expressed as follows:

$$C_p - C_v = R \quad (8)$$

From the aforementioned equation, the state equations of the pneumatic system can be

derived as follows:

$$\begin{cases} \dot{x}_1(t) = x_2(t) \\ \dot{x}_2(t) = \frac{A_v(t)(x_3(t) - x_4(t))\text{sgn}(x_2(t) - F_f)}{m} \\ \dot{x}_3(t) = \frac{kRT_s \frac{C_d C_m P_i}{\sqrt{T_s}} k_v u(t) + kRT_s \frac{C_d C_m A_v(t)}{\sqrt{T_s}} x_3(t) - kx_3(t) A_v x_2(t)}{A_v(t)x_1(t) + V_i} \\ \dot{x}_4(t) = \frac{-kRT_s \frac{C_d C_m P_i}{\sqrt{T_s}} k_v u(t) + kRT_s \frac{C_d C_m A_v(t)}{\sqrt{T_s}} x_4(t) + kx_4(t) A_v x_2(t)}{V_i - A_v(t)x_1(t)} \end{cases} \quad (9)$$

$$y(t) = x_1(t) \quad (10)$$

where x is the state vector of the system.

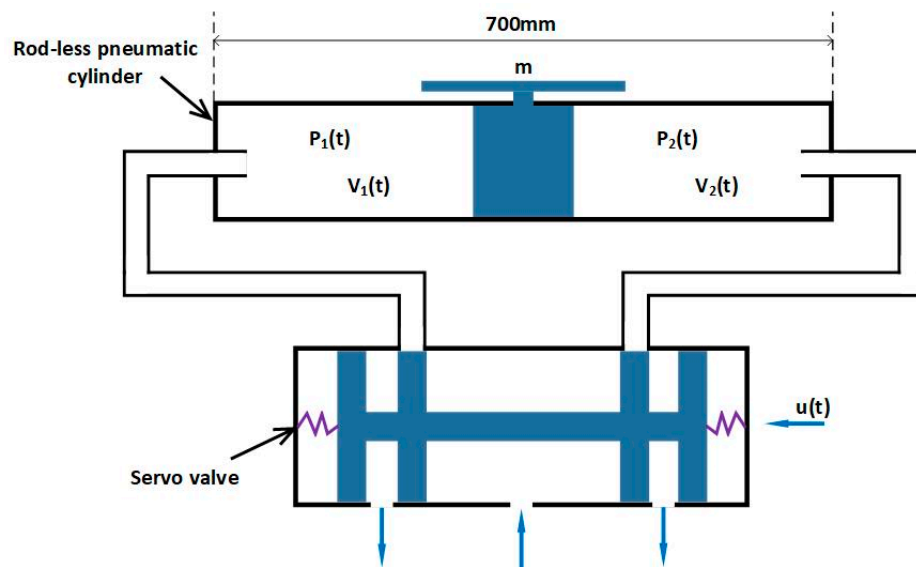


Figure 5. Schematic of the rod-less pneumatic cylinder and servo valve.

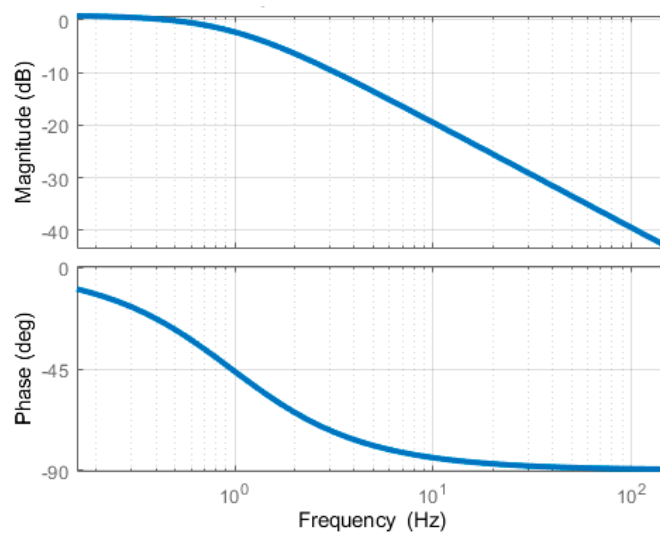


Figure 6. Bode diagram of a frequency response of the pneumatic valve.

3.2. Adaptive Sliding Mode Control [26,27]

To attain precise trajectory tracking control for a plug tray loading platform via the rod-less pneumatic cylinder, an adaptive sliding mode controller was devised. This controller

employed Fourier series approximation techniques as the orthogonal function sets to effectively handle nonlinearities, uncertainties and time variations in the mathematical models of the precision pneumatic plug tray seeder system. Any function that satisfies the Dirichlet conditions in the interval $[-P, P]$ can be expanded into a Fourier series as follows:

$$f(t) = a_0 + \sum_{n=1}^{\infty} \left[a_n \cos \frac{n\pi t}{P} + b_n \sin \frac{n\pi t}{P} \right] \tag{11}$$

where $a_0, a_n,$ and b_n are Fourier coefficients, which can be expressed as follows:

$$\begin{cases} a_0 = \frac{1}{2P} \int_{-P}^P f(t) dt \\ a_n = \frac{1}{P} \int_{-P}^P f(t) \cos \frac{n\pi t}{P} dt, n = 1, 2, 3, \dots \\ b_n = \frac{1}{P} \int_{-P}^P f(t) \sin \frac{n\pi t}{P} dt, n = 1, 2, 3, \dots \end{cases} \tag{12}$$

The function $f(t)$ can be approximated by products of a coefficient vector and an orthogonal function vector as follows:

$$f(t) \approx W^T Z(t) \tag{13}$$

$$W = [w_1 w_2 \dots w_n]^T \tag{14}$$

$$Z(t) = [Z_1 Z_2 \dots Z_n]^T \tag{15}$$

In SMC, the sliding plane must first be established. The tracking error $e(t)$ of a pneumatic system trajectory is defined as follows:

$$e(t) = y_m(t) - y(t) \tag{16}$$

where $y(t)$ is the system output and $y_m(t)$ is the reference trajectory. The sliding surface s is defined as follows:

$$s = a_1 e(t) + a_2 \dot{e}(t) + \ddot{e}(t) \tag{17}$$

where a_1 and a_2 are the parameters of the designed sliding surface. Given the aforementioned sliding surface and state equations of the pneumatic system, represented with a function approximation method, the control input of the designed adaptive sliding mode controller can be expressed as follows:

$$u(t) = \frac{-\widehat{W}_F^T Z_F(t) - e(t) - a_1 \dot{e}(t) - a_2 \ddot{e}(t) - p_{21} e(t) - p_{22} \dot{e}(t) + \ddot{y}_m(t) - \frac{s}{2\rho^2}}{\widehat{W}_g^T Z_g(t)} \tag{18}$$

This controller aims to minimize tracking errors and stabilize the system. Figure 7 shows a block diagram of an adaptive sliding mode controller. In (18), \widehat{W}_F and \widehat{W}_g are the coefficients calculated using the function approximation method to estimate the pneumatic system, Z_F and Z_g are the orthogonal function sets calculated using the function approximation method to estimate the pneumatic system, ρ is a positive parameter, and p_{21} and p_{22} are the elements of the adaptive parameter p , which can be expressed as follows:

$$A = \begin{bmatrix} 0 & 1 \\ a_1 & a_2 \end{bmatrix}, A^T p + pA = -Q, \quad Q \in \text{positive definite matrix} \tag{19}$$

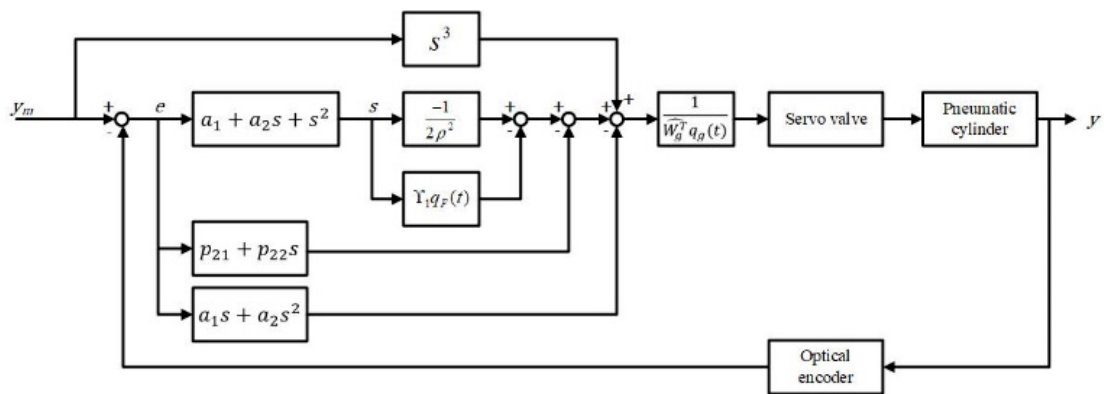


Figure 7. Block diagram of an adaptive sliding mode controller.

To demonstrate the stability of the controller, a Lyapunov candidate function V was introduced as Equation (20), and intelligent parameter adjustments were employed to adapt the controller. The derivative of the Lyapunov candidate function showed that the energy of the system decreased over time, indicating the stability.

$$V = \frac{1}{2} \left(s^2 + e^T p e + \tilde{W}_F^T \Upsilon_1^{-1} \tilde{W}_F + \tilde{W}_g^T \Upsilon_2^{-1} \tilde{W}_g \right) \tag{20}$$

where V is the total energy of the system, s^2 is the sliding surface, $e^T p e$ is the system error, and $\tilde{W}_F^T \Upsilon_1^{-1} \tilde{W}_F$ and $\tilde{W}_g^T \Upsilon_2^{-1} \tilde{W}_g$ are the system states. Here, $\tilde{W}_F = \hat{W}_F - W_F$, and $\tilde{W}_g = \hat{W}_g - W_g$, and an intelligent parameter adjustment is employed as follows:

$$\dot{\hat{W}}_F = \gamma_1 s q_F(t) \tag{21}$$

$$\dot{\hat{W}}_g = \gamma_2 s q_g(t) \tag{22}$$

where $\gamma_1 > 0$ and $\gamma_2 > 0$ are gain matrices. The derivative of V can be obtained as follows:

$$\dot{V} = s\dot{s} + \frac{1}{2} e^T \dot{p} e + \frac{1}{2} e^T p \dot{e} + \tilde{W}_F^T \gamma_1^{-1} \dot{\tilde{W}}_F + \tilde{W}_g^T \gamma_2^{-1} \dot{\tilde{W}}_g \tag{23}$$

By substituting (20)–(22) into (23), we obtain the following expression:

$$\dot{V} = -\frac{1}{2} \left(e^T Q_e + \left(\frac{s}{\rho} - \rho w_t \right)^2 - \rho^2 w_t^2 \right) \leq -\frac{1}{2} \left(e^T Q_e - \rho^2 w_t^2 \right) \tag{24}$$

Then, by integrating (24), we obtain the following expression:

$$V(t) \leq V(0) - \frac{1}{2} \int_0^t \left(e^T Q_e - \rho^2 w_t^2 \right) d\tau \tag{25}$$

where w_t is the actual upper limit of the approximation errors. According to Barblat’s lemma, $\dot{V}(t)$ is bounded for $t \geq 0$, indicating that $s \rightarrow 0$ and $e \rightarrow 0$ when $t \rightarrow \infty$. When $s \rightarrow 0$, the system will tend to be stable through the sliding surface. When $s = 0$, the sliding surface can be described as follows:

$$a_1 e(t) + a_2 \dot{e}(t) + \ddot{e}(t) = 0 \tag{26}$$

Using Laplace transform, (26) can be converted to s -domain:

$$a_1E(s) + a_2sE(s) + s^2E(s) = 0 \quad (27)$$

The open-loop transfer function $G(s)$ can be described as follows:

$$G(s) = \frac{a_2s + s^2}{a_1} \quad (28)$$

With final value theorem

$$\lim_{t \rightarrow \infty} g(t) = \lim_{s \rightarrow 0} sG(s) \quad (29)$$

(28) can be converted as follows:

$$\lim_{t \rightarrow \infty} e(t) = \lim_{s \rightarrow 0} \frac{s(a_2s + s^2)}{a_1} = 0 \quad (30)$$

According to (30), the tracking errors e would tend to 0 when $t \rightarrow \infty$ can be proven. By applying the final value theorem, it was proven that the tracking errors would tend to zero as time approached infinity, confirming the system to stabilize and accurately track the reference trajectory through the designed adaptive sliding mode controller.

4. Results and Discussions

4.1. Simulations

To ensure the feasibility of the precision pneumatic plug tray seeder, trajectory tracking simulations of the proposed pneumatic system was conducted using MATLAB. A fifth-order polynomial trajectory was used as the reference trajectory for trajectory tracking control, which was combined with the established mathematical model and the proposed controller described in Section 3. To objectively evaluate the performance of the controller, the *RMSE* was defined as follows:

$$RMSE = \sqrt{\frac{1}{N} \sum_{k=N_1}^{N_2} e_k^2} \quad (31)$$

where $N = N_2 - N_1$, with N_1 representing the starting time and N_2 representing the ending time.

Figure 8 shows the open-loop experimental results of the rod-less pneumatic cylinder at an input signal of 6 V. The blue line and the red line in Figure 8a represent cylinder trajectories of the simulation and the experiment, respectively. To increase the consistency between the simulation and experimental results, the simulation parameters were adjusted in the open-loop experiment. Figure 9 depicts the trajectory tracking simulation results of the proposed adaptive sliding mode controller with a reference fifth-order polynomial trajectory of 200 mm/4 s. According to these simulation results, the proposed controller exhibited excellent trajectory tracking performances, with an *RMSE* of 0.185 mm and a maximum error of 0.874 mm.

Figures 10 and 11 illustrate the sliding surface s and the phase plane of $e(t)$ and $\dot{e}(t)$ based on the trajectory tracking simulation results in Figure 9, respectively. It is seen that the sliding mode is in the reaching phase for the first 0.3 s, and then enters the sliding phase. When the tracking error is smaller, the sliding surface is closer to 0. In the phase plane, tracking errors successfully converge to the origin, confirming the stability of the system [28].

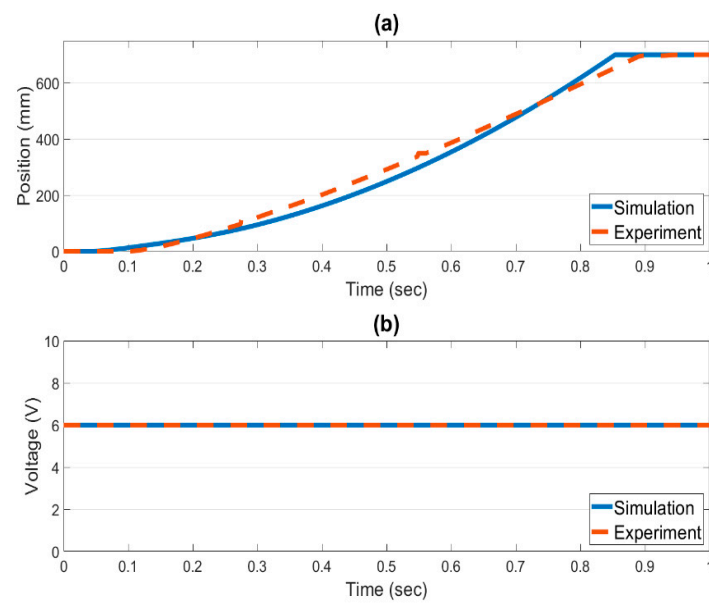


Figure 8. Results of the open-loop experiment: (a) cylinder trajectories and (b) control signals.

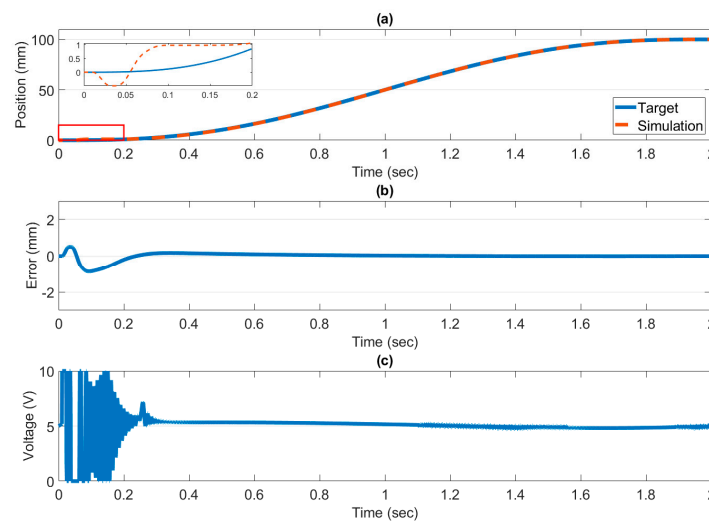


Figure 9. Simulation results: (a) cylinder trajectories, (b) tracking errors, and (c) control signals.

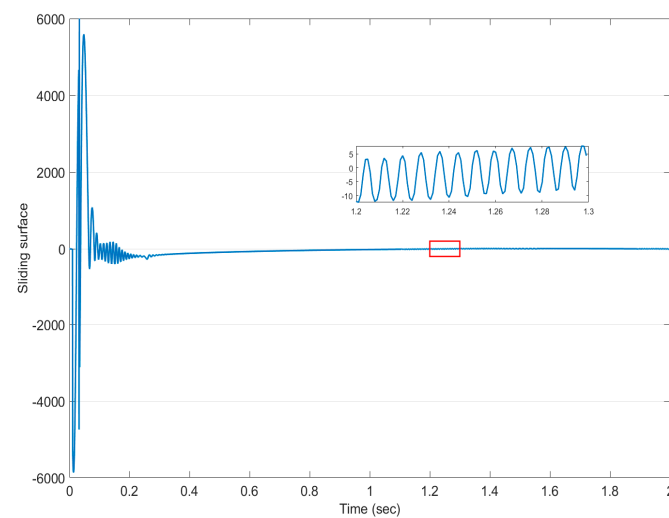


Figure 10. The sliding surface of the system.

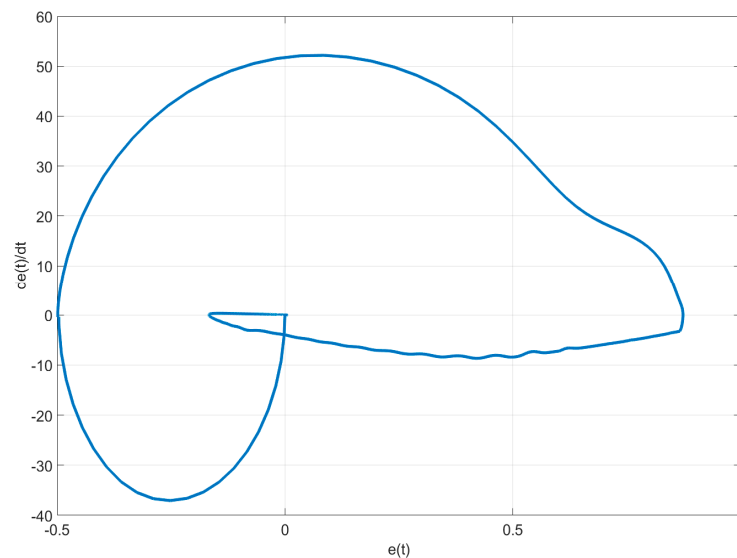


Figure 11. The phase plane of the system.

4.2. Experiments

The precision pneumatic plug tray seeder developed in this study is compatible with a variety of plug trays, and the proposed plug tray loading platform primarily consists of rod-less pneumatic cylinders. To ensure that the seeds fall at the center of the tray cell, precise control of the pneumatic cylinder's trajectory is required. In this study, a PC-based real-time trajectory tracking control platform was established using MATLAB/SIMULINK, and an adaptive sliding mode controller was proposed. Controller performance was verified through trajectory tracking experiments with varying strokes and speeds. Figures 12 and 13 depict the experimental results of the plug tray loading platform for both a fifth-order polynomial trajectory at 500 mm/10 s and a hybrid trajectory, which was a combination of a fifth-order polynomial trajectory at 500 mm/10 s and a $25 \times \sin(2\pi \times 0.32 \times t)$ trajectory, with RMSEs of 0.769 and 0.570 mm and maximum errors of 2.729 and 2.107 mm, respectively. Figure 14 shows the experimental results of the seeding trajectory for the plug tray loading platform, with an RMSE of 0.436 mm and a maximum error of 2.357 mm. The seeding trajectory was established using a 104-cell plug tray with a center distance of 42 mm and a seeding speed of 60 s/tray. Figure 15 displays the operational status of various components in the precision pneumatic plug tray seeder. Solenoid valves were used to control the guided drives of each component by 0–5 V control signals. In coordination with speeds of the plug tray loading platform, the lengths of operation time for the soil drilling mechanism are 2.15 s. After soil drilling, the seed picking mechanism was used for 1.7 s to pick up seeds. Finally, the seeding mechanism operated for 1.35 s, with vacuum generators operating for 3.125 s to drop seeds. The success of seed suction directly affects seeding performances. In the trajectory experiments, all RMSEs were less than 1 mm, and none of the maximum errors exceeded 3 mm. This process ensured the accuracy of the precision pneumatic plug tray seeder during seeding and also guaranteed its adaptability to different plug tray sizes and seeding speeds. Table 3 compares multiple control methods with trajectory tracking experiments involving pneumatic cylinders for fifth-order polynomial trajectory, hybrid trajectory and seeding trajectory comparing with the control methods in [23,24], and smaller RMSEs of our control methods were achieved. Also, Figure 16 shows the scatter plot of reliabilities for RMSE-Maximum errors via ten replicates in three different trajectories we proposed in this study. Experimental results show that the proposed controller exhibited satisfactory performances.

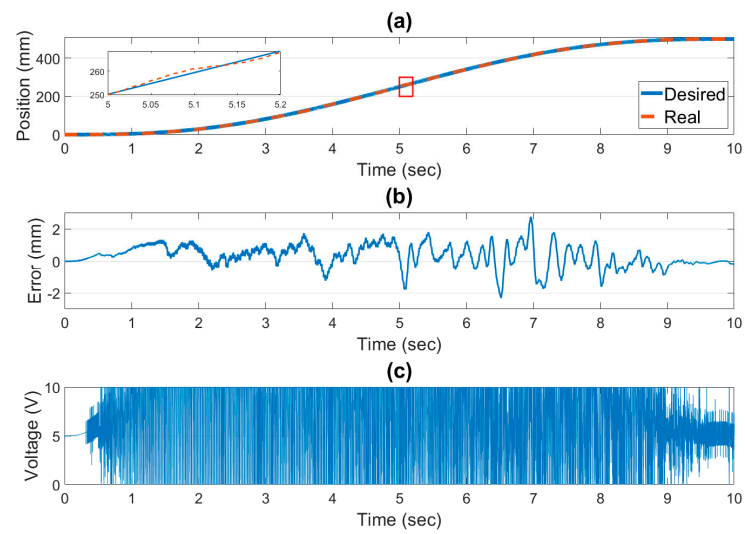


Figure 12. Experimental results: (a) cylinder trajectories, (b) tracking errors, and (c) control signals.

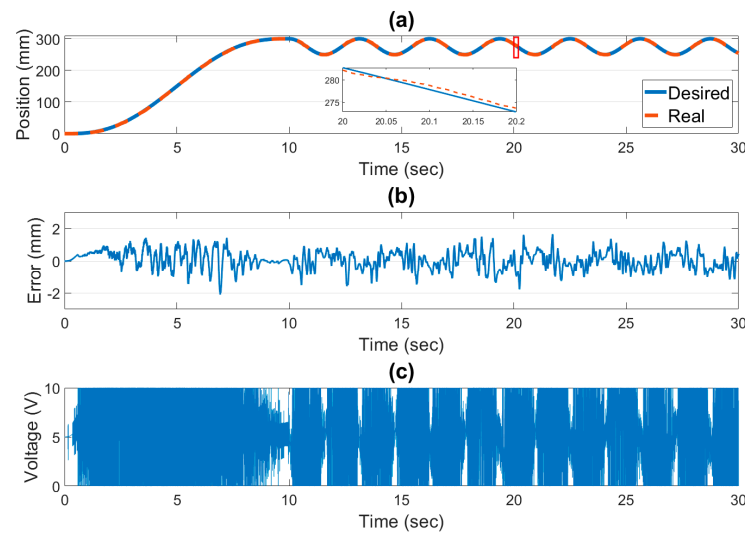


Figure 13. Experimental results: (a) cylinder trajectories, (b) tracking errors, and (c) control signals.

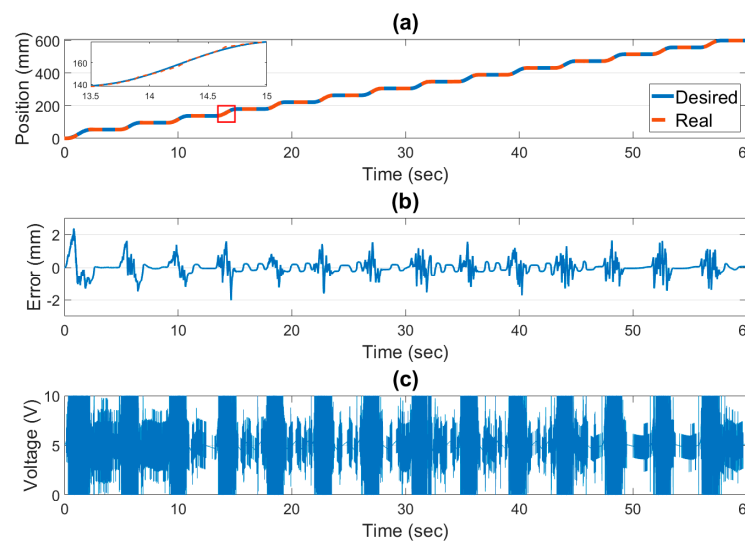


Figure 14. Experimental results: (a) cylinder trajectories, (b) tracking errors, and (c) control signals.

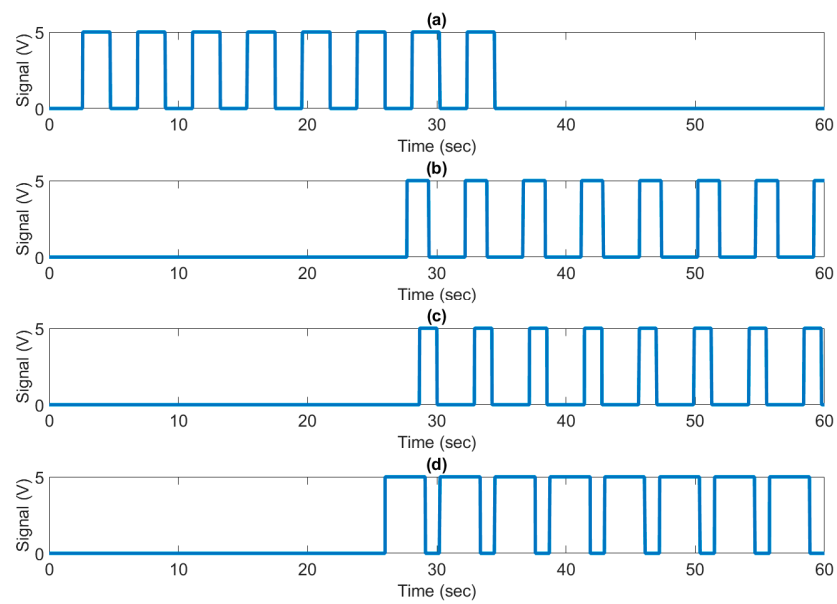


Figure 15. Operation times of the (a) soil drilling mechanism, (b) picking mechanism, (c) seeding mechanism, and (d) vacuum generators.

Table 3. Comparisons of control methods.

Control Method	Trajectory	RMSE (mm)	Max. Error (mm)
Proposed method	Fifth-order polynomial trajectory	0.769	2.729
Proposed method	Hybrid trajectory	0.570	2.107
Proposed method	Seeding trajectory	0.436	2.357
Method in Ref. [23]	Sine trajectory	1.037	-
Method in Ref. [23]	Multi-frequency sine trajectory	0.831	-
Method in Ref. [24]	Sine trajectory	9.82	-

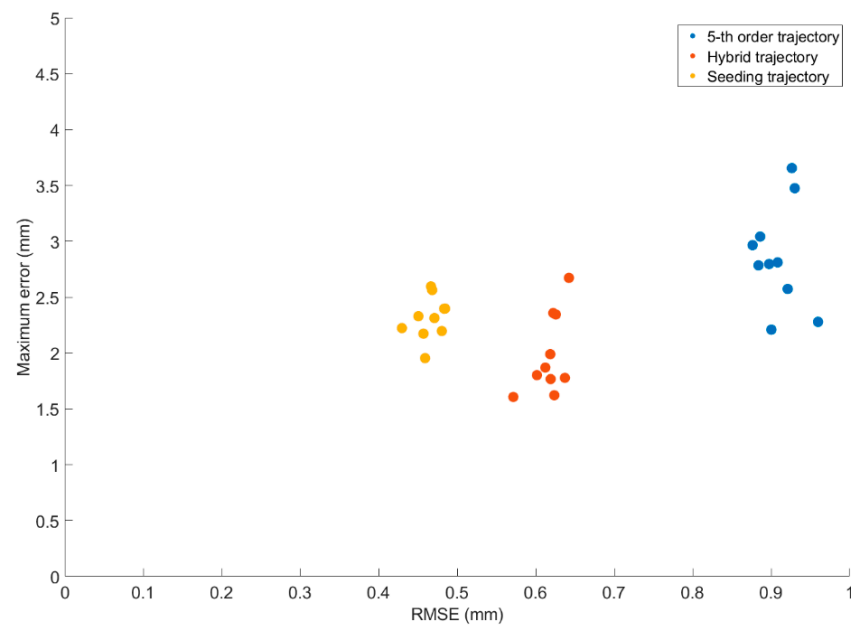


Figure 16. The scatter plot of reliabilities for RMSE-Maximum errors in various trajectories.

4.3. Seeding Rate Analysis

Seeding one seed per cell of a plug tray is the optimal method for seedling development. In this study, seeding rates were analyzed to investigate the performance of the

proposed precision pneumatic plug tray seeder. While, single seeding is defined as seeding only one seed in a plug tray cell, multiple seeding is defined as seeding two or more seeds in a plug tray cell, and missed seeding is defined as not seeing any seeds in a plug tray cell. The optimal conditions for seed suction have been verified through experiments. The main influencing factor is the inner diameter of the suction needle; needles of 0.51 mm inner diameter were selected in this study. Providing enough vacuum pressure can ensure that seeds are stably adsorbed. Table 4 lists the seeding experimental results of the precision pneumatic plug tray seeder, which were obtained by conducting the experiment three times under the same conditions. Through these repeated experiments, the optimal experimental conditions were determined to be a seeding speed of 60 s/tray, a vacuum pressure of -0.65 bar, and a needle inner diameter of 0.51 mm. Multiple cruciferous seeds were tested. The single-seeding rates were all above 94%, with multiple-seeding rates not exceeding 5%. However, compared with the multiple-seeding rate, the missed-seeding rate was more concerning. According to the experimental results, the missed-seeding rates of the precision pneumatic plug tray seeder did not exceed 4%.

Table 4. Comparison of Seeding methods.

Seeding Method	Crop	Single-Seeding Rate (%)	Multi-Seeding Rate (%)	Missed-Seeding Rate (%)	Germination Rate (%)
Proposed method	<i>Brassica rapa</i> subsp. <i>pekinensis</i>	94.23	0.32	3.21	94.23
Proposed method	<i>Brassica rapa</i> subsp. <i>chinensis</i>	94.87	4.49	0.64	83.01
Proposed method	<i>Brassica parachinensis</i>	97.12	0.96	1.92	95.83
Proposed method	<i>Brassica oleracea</i> var. <i>botrytis</i>	95.20	1.92	2.88	87.18
Proposed method	<i>Brassica oleracea</i> var. <i>capitata</i>	96.48	2.56	0.96	91.35
Method in Ref. [1]	Capsicum	92.46	5.23	2.31	-
Method in Ref. [1]	Tomato	90.12	6.4	3.48	-

The proposed precision pneumatic plug tray seeder not only offered precise seeding but also demonstrated excellent results in the seeding rate experiments. Therefore, to determine whether seeding with the proposed precision pneumatic plug tray seeder affected seed growth, a germination experiment was conducted. Table 4 shows the results of this germination experiment, which was conducted three times under the same conditions. After the proposed precision pneumatic plug tray seeder was used for seeding, the plug trays were placed in a well-illuminated space for cultivation and watered twice a day with 5 mL of water per cell. Figure 17 shows the results of the germination experiments for *Brassica rapa* subsp. *pekinensis*, *Brassica rapa* subsp. *chinensis*, *Brassica oleracea* var. *botrytis*, *Brassica oleracea* var. *botrytis*, and *Brassica oleracea* var. *capitata*. According to the experimental results, the germination rate of all the crop seeds exceeded 95%, which is almost identical to that of manual seeding; this result confirmed that the precision pneumatic plug tray seeder did not affect seed growth.

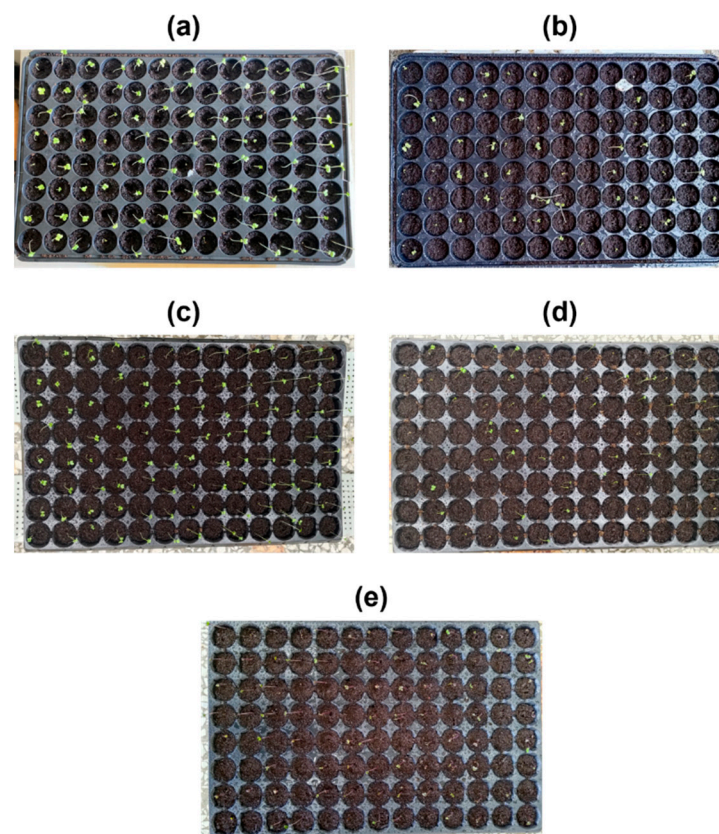


Figure 17. Results of the germination experiment for (a) *Brassica rapa* subsp. *pekinensis*, (b) *Brassica rapa* subsp. *chinensis*, (c) *Brassica oleracea* var. *botrytis*, (d) *Brassica oleracea* var. *botrytis*, and (e) *Brassica oleracea* var. *capitata*.

5. Conclusions

In this study, a precision pneumatic plug tray seeder was developed by applying a pneumatic servo system to an automatic plug tray, which consisted of a plug tray loading platform and a seeding system. A PC-based real-time control platform was established for trajectory tracking through MATLAB/SIMULINK, and an adaptive sliding mode controller was proposed to precisely control the trajectory of the pneumatic cylinder. The performance of the system was then evaluated through trajectory tracking experiments with multiple strokes and speeds. According to the experimental seeding results, all single-seeding rates exceeded 97%, while missed-seeding rates did not exceed 4%. The system exhibited high adaptability to different plug tray sizes and seeding speeds, thereby confirming its accuracy during seeding.

Overall, the proposed adaptive sliding mode controller exhibited high trajectory tracking performance, with an RMSE of 0.436 mm and a maximum error of 2.107 mm. Compared with other control methods, the proposed controller exhibited satisfactory performance. Therefore, the proposed controller appears to be suitable for agricultural production, especially in the plug tray seeding industry.

Author Contributions: Conceptualization, H.-T.L.; methodology, H.-T.L.; software, H.-T.L. and Y.-H.L.; validation, H.-T.L. and Y.-H.L.; data curation, Y.-H.L.; writing—original draft preparation, H.-T.L. and Y.-H.L.; writing—review and editing, H.-T.L.; supervision, H.-T.L. All authors have read and agreed to the published version of the manuscript.

Funding: This research was sponsored by National Science and Technology Council, Taiwan under the grant MOST 111-2221-E-005-082.

Data Availability Statement: Data sharing is not applicable to this article.

Conflicts of Interest: The authors declare no conflict of interest.

References

1. Gaikwad, B.B.; Sirohi, N.P.S. Design of a low-cost pneumatic seeder for nursery plug trays. *Biosyst. Eng.* **2008**, *99*, 322–329. [[CrossRef](#)]
2. EL-Ghobashy, H.; Mohamed, T.; EL-Ashker, A.; Shabaan, Y. Development of a locally vacuum vegetable seeder for nursery trays. *J. Soil Sci. Agric. Eng.* **2016**, *7*, 595–602. [[CrossRef](#)]
3. Naik, M.D.A.; Thakur, H.M. Design and analysis of an automated seeder for small scale sowing applications for tray plantation method. *Int. J. Eng. Res. Technol.* **2017**, *10*, 716–723.
4. Xia, H.; Zhen, W.; Liu, Y.; Zhao, K. Optoelectronic measurement system for a pneumatic roller-type seeder used to sow vegetable plug-trays. *Measurement* **2021**, *170*, 108741. [[CrossRef](#)]
5. Karayel, D.; Barut, Z.; Özmerzi, A. Mathematical modelling of vacuum pressure on a precision seeder. *Biosyst. Eng.* **2004**, *87*, 437–444. [[CrossRef](#)]
6. Xia, H.; Liu, Y.; Zhao, K.; Jiang, L.; He, Z.; Gu, S. A novel sowing operation parameter learning optimization method using dataset of sown seeds with similar properties. *Comput. Electron. Agric.* **2022**, *201*, 107293. [[CrossRef](#)]
7. Pareek, C.M.; Tewari, V.K.; Machavaram, R. Multi-objective optimization of seeding performance of a pneumatic precision seed metering device using integrated ANN-MOPSO approach. *Eng. Appl. Artif. Intell.* **2023**, *117*, 105559. [[CrossRef](#)]
8. Li, Z.; Wu, J.; Du, J.; Duan, D.; Zhang, T.; Chen, Y. Experimenting and Optimizing Design Parameters for a Pneumatic Hill-Drop Rapeseed Metering Device. *Agronomy* **2023**, *13*, 141. [[CrossRef](#)]
9. Silva, G.N.; de Pinho, M.D.R.; Teixeira, M.A.; Messias, M.; Macau, E. Nonlinear Systems: Asymptotic Methods, Stability, Chaos, Control, and Optimization. *Math. Probl. Eng.* **2011**, *2011*, 498751. [[CrossRef](#)]
10. Moriwaki, K. A Harvest Vehicle with Pneumatic Servo System for Gathering a Harvest and its Control. *IFAC-Pap.* **2016**, *49*, 460–466. [[CrossRef](#)]
11. Lin, W.; Guan, R.; Yuan, L.; Li, Z.; Tong, M. Position feedback dynamic surface control for pneumatic actuator position servo system. *Syst. Sci. Control Eng.* **2018**, *6*, 388–397. [[CrossRef](#)]
12. Zhang, Y.; Li, K.; Wang, G.; Liu, J.; Cai, M. Nonlinear model establishment and experimental verification of a pneumatic rotary actuator position servo system. *Energies* **2019**, *12*, 1096. [[CrossRef](#)]
13. Gao, H.; Kareem, A.; Jawarneh, M.; Ofori, I.; Raffik, R.; Kishore, K.H. Metaheuristics Based Modeling and Simulation Analysis of New Integrated Mechanized Operation Solution and Position Servo System. *Math. Probl. Eng.* **2022**, *2022*, 1466775. [[CrossRef](#)]
14. Zhang, B.; Jiang, A.; Jiang, J.; Qi, Y.; Xue, L.; Wang, Y. A New Positioning Strategy Based on Parameter Tuning and Optimal Control Technique for Pneumatic Control Valve. *Actuators* **2022**, *11*, 279. [[CrossRef](#)]
15. Wang, Z.; Guo, Z.; Zhu, G.; Wang, X.; Li, X. Finite Element Modeling and Optimal Design of an Electromagnetic Pneumatic Flow Servo Valve. *Math. Probl. Eng.* **2023**, *2023*, 2796963. [[CrossRef](#)]
16. Zhu, M.; Chen, S.; Xu, Z.; Dong, X. Design of Two-Degree-of-Freedom Fractional-Order Internal Model Control Algorithm for Pneumatic Control Valves. *Actuators* **2023**, *12*, 214. [[CrossRef](#)]
17. Ding, S.; Park, J.H.; Chen, C.C. Second-order sliding mode controller design with output constraint. *Automatica* **2020**, *112*, 108704. [[CrossRef](#)]
18. Fei, J.; Wang, Z.; Liang, X.; Feng, Z.; Xue, Y. Fractional sliding-mode control for microgyroscope based on multilayer recurrent fuzzy neural network. *IEEE Trans. Fuzzy Syst.* **2021**, *30*, 1712–1721. [[CrossRef](#)]
19. Li, F.; Zhang, Z.; Wu, Y.; Chen, Y.; Liu, K.; Yao, J. Improved fuzzy sliding mode control in flexible manipulator actuated by PMAs. *Robotica* **2022**, *40*, 2683–2696. [[CrossRef](#)]
20. Yu, L.; Huang, J.; Luo, W.; Chang, S.; Sun, H.; Tian, H. Sliding-Mode Control for PMLSM Position Control—A Review. *Actuators* **2023**, *12*, 31. [[CrossRef](#)]
21. Chen, G.; Jiang, Y.; Tang, Y.; Xu, X. Revised adaptive active disturbance rejection sliding mode control strategy for vertical stability of active hydro-pneumatic suspension. *ISA Trans.* **2023**, *132*, 490–507. [[CrossRef](#)] [[PubMed](#)]
22. Sun, Z.; Hu, S.; Xie, H.; Li, H.; Zheng, J.; Chen, B. Fuzzy adaptive recursive terminal sliding mode control for an agricultural omnidirectional mobile robot. *Comput. Electr. Eng.* **2023**, *105*, 108529. [[CrossRef](#)]
23. Ren, H.P.; Wang, X.; Fan, J.T.; Kaynak, O. Fractional order sliding mode control of a pneumatic position servo system. *J. Frankl. Inst.* **2019**, *356*, 6160–6174. [[CrossRef](#)]
24. Zhao, L.; Gu, S.; Zhang, J.; Li, S. Finite-time trajectory tracking control for rodless pneumatic cylinder systems with disturbances. *IEEE Trans. Ind. Electron.* **2021**, *69*, 4137–4147. [[CrossRef](#)]
25. Available online: <https://www.festo.com/gb/en/a/532641/?q=~:sortByFacetValues-asc> (accessed on 20 July 2023).
26. Lin, H.T. A novel real-time path servo control of a hardware-in-the-loop for a large-stroke asymmetric rod-less pneumatic system under variable loads. *Sensors* **2017**, *17*, 1283. [[CrossRef](#)] [[PubMed](#)]
27. Lin, H.T. Development of the Intelligent Pneumatic Sewing Platform for Mask Production. *IEEE Access* **2020**, *8*, 141777–141786. [[CrossRef](#)]
28. Eker, I. Second-order sliding mode control with experimental application. *ISA Trans.* **2010**, *49*, 394–405. [[CrossRef](#)]

Disclaimer/Publisher’s Note: The statements, opinions and data contained in all publications are solely those of the individual author(s) and contributor(s) and not of MDPI and/or the editor(s). MDPI and/or the editor(s) disclaim responsibility for any injury to people or property resulting from any ideas, methods, instructions or products referred to in the content.